Chapter 4
Anode Material Selection and Design Issues

"All that glitters is not gold, but at least it contains free electrons." -Author Unknown

Included in this chapter are discussions of the processes, tests, and results used to select the anode material for VTPT-3. Traditionally, tungsten has been a widely accepted electrode material for plasma torches and was used for the anode on all previous Virginia Tech torches. However, although pure tungsten offers excellent material properties as an electrode, the size and complex design of the current anode discourages using a material that is difficult to machine. In addition, the studies presented here are for uncooled anodes. It is recognized that active cooling of the anode can significantly increase the lifetime of an anode material, but the goal here is to investigate the fundamental processes of electrode erosion based solely on material properties. Three anode materials were tested in a quiescent environment: pure copper, a 70/30 tungsten-copper alloy, and pure molybdenum. These metals were identified as having desirable properties for this type of application. Two criteria, anode lifetime and arc stability, were chosen to form the basis of material selection. Evaluations of how materials met these criteria were made through observations of torch performance, measurement of the anode volumetric loss, and a stereoscopic investigation of the arc attachment region after each test. Based on the results of the experimental tests, molybdenum was selected as the material for all future VTPT-3 anodes because of its long operational lifetime, low anode volumetric loss, and stability of operation. Another observation was that air and nitrogen plasmas are quite erosive to molybdenum. When these plasmas are used, copper is a good substitute for molybdenum.

To support the experimental tests, an analytical model was developed to predict the diameter of the arc attachment point on the anode. For a given current, the arc diameter determines the local heat flux incident on the anode, which consequently affects the rate of electrode erosion. So, in essence, the model predicts the rate of electrode erosion indirectly through an analysis of the arc diameter at the anode surface. This model is capable of allowing input changes for the anode thermionic work function, operating temperature, thermal conductivity, and the thermal conductivity of the electrons

in the anode fall region. Other parameters in the model, such as plasma temperature and anode thickness, were held constant. The results were plotted against arc current to determine if some materials performed better in certain operating regimes. Over the entire range of currents, the model predicted molybdenum would provide the best mix of material properties for this application, matching the experimental results quite well.

Once the anode material was selected based on the quiescent and analytical studies, stereoscopic investigations of crossflow, exit geometry, and feedstock type were performed to determine how the arc attachment point was affected by these parameters. The crossflow study involved a torch with a molybdenum anode designed for normal injection into a supersonic crossflow. Stereoscopic investigations showed that, in almost all cases, the crossflow forced the arc to attach on the downstream side of the anode constrictor. Two anodes with elliptical exits designed for angled injection showed a different trend. In these cases, the arc attached on the side of the constrictor, or on the upstream side, producing the minimum possible arc length. Finally, stereoscopic investigations of molybdenum anodes after operation on hydrocarbon, nitrogen, and air plasmas showed that air and nitrogen plasmas are quite erosive to molybdenum. This prompted a switch to copper when air or nitrogen feedstocks were used. Under these circumstances, the copper anodes lasted much longer than the molybdenum anodes.

4.1: Material Review and Selection Criteria

The following is a short discussion of important material properties used for selecting an anode material and supports the choices to test the chosen three anode materials. For the anode, the most important material properties to be investigated are the melting point, electrical conductivity, thermionic work function, heat transfer coefficient, and hardness. These properties, through various physical means, affect the diameter of the arc attachment point on the anode surface. The diameter of the arc attachment point determines the local heat flux to the anode, which directly affects the rate of erosion as the anode metal vaporizes. Ideally, a desirable combination would be one that provides for an anode with a high operating temperature, causing the arc diameter to increase, but not so high that it causes vaporization. In addition, the overall bulk of the anode must be considered, as it contributes to the thermal resistance of the anode. These properties and

their effect on the arc diameter are discussed in more detail in Section 4.3.3. Certainly cost is an issue as well, which was why rhenium, a metal with excellent material properties and exceptional corrosion resistance to air plasma, was not chosen, as it costs $300 per ounce.

Traditionally, tungsten has been a widely accepted choice for electrodes, as it has a desirable mix of material properties such as high melting temperature and hardness, good electrical conductivity through a wide temperature range, and good corrosion resistance to certain plasmas. Molybdenum is quite comparable to tungsten in many respects, owing to a similar body-centered-cubic structure. Although molybdenum has a lower melting temperature than tungsten, it is easier to machine and costs about 30% less. Copper is very soft compared to other metals and has extremely low electrical resistivity of 1.7×10^{-8} Ωm, about 65% lower than either tungsten or molybdenum. In addition, although other metals may offer a better overall mix of material properties, copper is quite cheap and has better corrosion resistance to air plasmas than either tungsten or molybdenum. Table 4.1 outlines a few of the material properties of these three metals, with some short notes for each.

Table 4.1: Table of Material Properties

Metal:	Melting Point (K)	Mineral Hardness	Comments:
Tungsten	3800	7.5	Very hard, good corrosion resistance, maintains properties to high temperature, BCC structure.
Molybdenum	2890	5.5	Brittle, weak against excited nitrogen, similar to tungsten in many respects, BCC structure.
Copper	1350	3.0	Cheap, excellent electrical conductivity, very soft, causing galling, CCP structure.

4.2: Test Procedure

All of the electrode erosion tests were conducted in a quiescent environment with the plasma torch in a horizontal position operating on methane. A single machinist manufactured all the anodes to the same specifications, so that the anode geometry would not affect the results. Torch chamber pressure and current were held constant at 445 kPa and 23 A, respectively. Although the current appears somewhat arbitrary, Cobine (1941) notes that for high-current electric arcs above 10 A, anode current density becomes nearly constant, so tests conducted above this limit should be representative of tests under other

high-current conditions. Ignition was initiated using a high frequency burst. Upon ignition a timer was started to record the test duration.

Tests were scheduled to run for five minutes of continuous operation. Previous research showed that a majority of anode wear occurs during startup (Miller and Winstead, 1996), so if the torch blew out it would not be relit, as this would skew the results. During operation, qualitative observations were made on the stability of the torch and the lifetime of the anode. The anodes and cathodes were cleaned and weighed before and after each test to determine the mass loss. Volumetric losses were calculated by dividing the mass loss by the known material densities. Volumetric losses are considered more representative of anode wear since denser materials may exhibit more mass loss, but volumetrically lose less material. Once the volumetric losses were calculated, photograph pictures of the wear regions were taken using a stereoscope. This provided a detailed, close-up view of the arc attachment point(s) and provided a better understanding of where the arc attaches and the nature of the mass loss made through the calculations.

4.3: Results and Discussion

Based on the observed lifetime and the volumetric loss results, molybdenum was chosen as the new material with which to manufacture future anodes for VTPT-3. In addition, the model also predicted that of the three candidates, molybdenum would be the best choice. It should be noted here that the results presented here are for uncooled anodes and may not extend to anodes with active cooling. Although molybdenum anodes experienced slightly higher volumetric loss rates than tungsten-copper anodes, only the molybdenum anodes lasted the full five-minute test period. Copper was rejected for its poor performance, both for its short lifetime and its high volume loss. However, during the testing it was observed that nitrogen plasmas are quite erosive to molybdenum, so under these circumstances copper is a good substitute, particularly when the test duration is short. Endurance testing in a supersonic tunnel showed that molybdenum anodes are quite durable and can withstand a grueling test cycle before needing to be replaced.

4.3.1: Quiescent Electrode Erosion Results

The results and conditions of the quiescent electrode erosion tests are shown in Table 4.2 for the anodes and Table 4.3 for the corresponding cathodes. Anodes are identified by material and number, such as molybdenum-1. A majority of the total electrode mass loss, about 70%, was confined to the anode. Referring to Table 4.2, it is clear that a marked difference exists between the volumetric material loss rates for copper and the other two anode materials. The average volumetric loss rate for copper anodes was 7.8×10^{-3} mm^3/sec, whereas the molybdenum and tungsten-copper anodes experienced average losses of 2.7×10^{-3} mm^3/sec and 1.7×10^{-3} mm^3/sec, respectively. Although the number of anodes used was limited by time and cost constraints, it is clear that there is a large performance deficit for copper anodes.

Regardless of the volumetric losses incurred during testing, the true merit of an anode material is determined by how long the anode lasts. Both of the molybdenum anodes endured the entire test period with few signs of instability. However, the tungsten-copper anodes have a mixed performance. Tungsten-copper-1 lasted the full test period, operating smoothly like the molybdenum, but tungsten-copper-2 extinguished shortly after two minutes had elapsed. This kind of varied performance produces uncertainty about the feasibility of using tungsten-copper anodes, regardless of whether or not the volumetric loss rates are slightly lower. Copper, on the other hand, had predictably poor performance. The three copper anodes (1, 2, and 3) lasted an average of two minutes. This average was boosted by the performance of copper-2, lasting almost four minutes. From an electrode lifetime perspective, molybdenum appears to have excellent durability and stable performance, necessary qualities for an anode material.

Table 4.2: Anode Erosion Test Results

Electrode Material	Average Current (A)	Run Time (sec)	Mass Loss (mg)	Erosion Rate (mg/min)	Volumetric Erosion Rate (mm^3/sec)
Molybdenum-1	23	300	10	2.0	3.3×10^{-3}
Molybdenum-2	23	300	6	1.2	2.0×10^{-3}
Tungsten-Copper-1	23	300	10	2.0	2.2×10^{-3}
Tungsten Copper-2	23	127	3	1.4	1.6×10^{-3}
Copper-1	24	99	6	3.6	6.7×10^{-3}
Copper-2	23	235	14	3.6	6.7×10^{-3}
Copper-3	23	45	4	5.3	9.9×10^{-3}

Table 4.3: Cathode Erosion Test Results

Electrode	Corresponding Anode	Average Power (W)	Mass Loss (mg)	Volumetric Erosion Rate (mm^3/sec)
Cathode 1	Molybdenum-1	1780	4	6.9×10^{-4}
Cathode 2	Molybdenum-2	1800	4	6.9×10^{-4}
Cathode 3	Tungsten-Copper-1	1800	3	5.2×10^{-4}
Cathode 4	Tungsten Copper-2	1880	4	1.6×10^{-3}
Cathode 5	Copper-1	2000	2	1.0×10^{-3}
Cathode 6	Copper-2	2070	4	8.7×10^{-4}
Cathode 7	Copper-3	1800	1	1.1×10^{-3}

Average erosion rate: 1.1 mg/min. Note: The average power presented in this table corresponds to the current listed in Table 4.2 for the anodes.

4.3.2: Stereoscopic Investigation of the Anodes and Cathodes

The stereoscopic investigation of the cathodes, and particularly the anodes, proved very interesting. Features unseen by the naked eye were observed and provided information about arc attachment, electrode erosion, and material properties.

4.3.2.1: Tungsten-Copper

Shown in Figures 4.1a and 4.1b are close-up photographs of the two tungsten-copper anodes after testing. In Figure 4.1a, a very deep cavity (1), penetrating about half the length of the anode constrictor, can be clearly seen at the bottom section of the constrictor exit. Lumps of once-molten tungsten have been deposited in the bottom of the cavity (2), identified by their highly reflective silver-colored surface. It appears as if all of the copper that originally occupied the cavity has been vaporized and ejected by the feedstock gas. Some short spires may be seen bordering the cavity (3). These are formed though convective forces and appear to consist mostly of copper. Finally, a well-defined region of heat treatment removal exists, characterized by the discoloration of the tungsten-copper alloy (4).

Tungsten-copper-2, shown in Figure 4.1b, exhibits a much different landscape. Instead of a large cavity, there is a much smaller cavity at the lip of the constrictor exit (1), approximately one-fifth as deep as the one shown in Figure 4.1a. In addition, two very interesting "drip" formations appear inside the constrictor (2 and 3). The mixed color of both drips suggests that they are made of the alloyed material. The largest one (2) originates at the base of the cavity and extends up, past the constrictor exit. This formation appears to have become molten and then convectively formed by the flowing

methane feedstock before cooling and solidifying. The second drip formation, which also originates at the base of the cavity, extends down into the constrictor. It is approximately one-fourth the size of the larger drip formation. How this feature was formed is a mystery, as gravitational effects did certainly not cause it, given that the torch was horizontal, or through convective forces, since the feedstock gas flowed in the opposite direction and was not shut off until several seconds after the arc was extinguished.


(a) Tungsten-Copper-1   (b) Tungsten-Copper-2
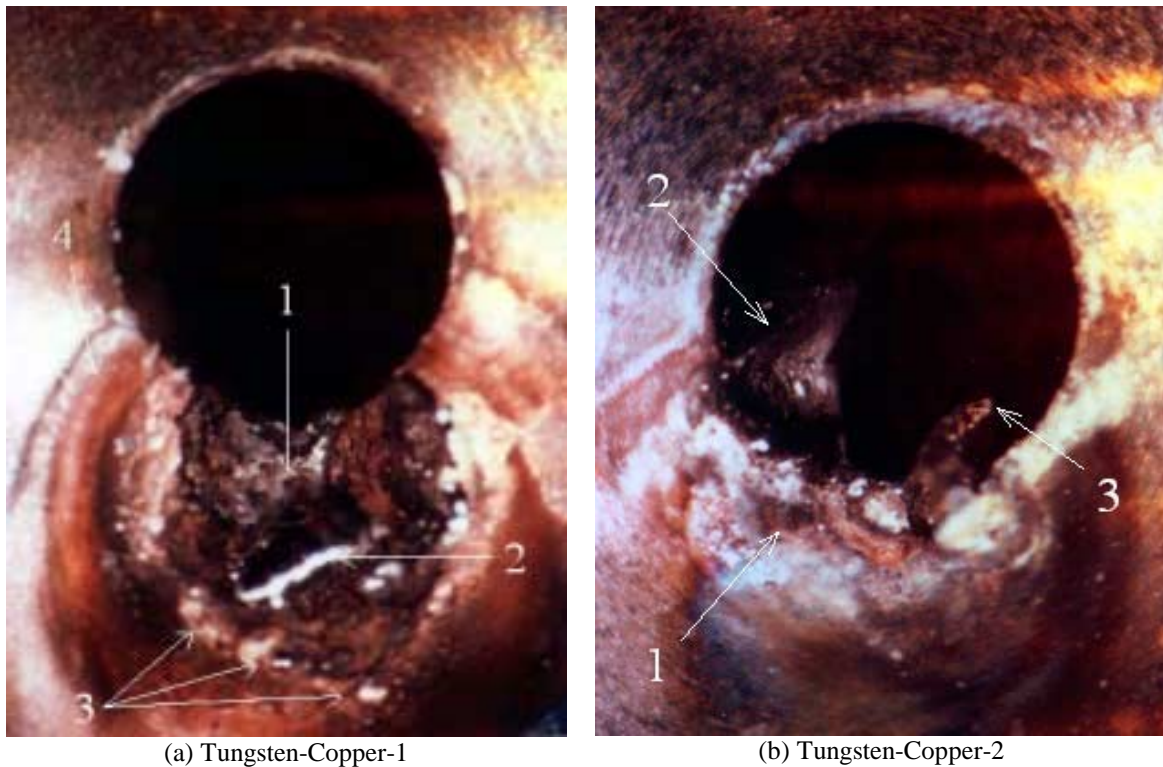
Figure 4.1: Stereoscopic Photographs of Worn Tungsten-Copper Anodes
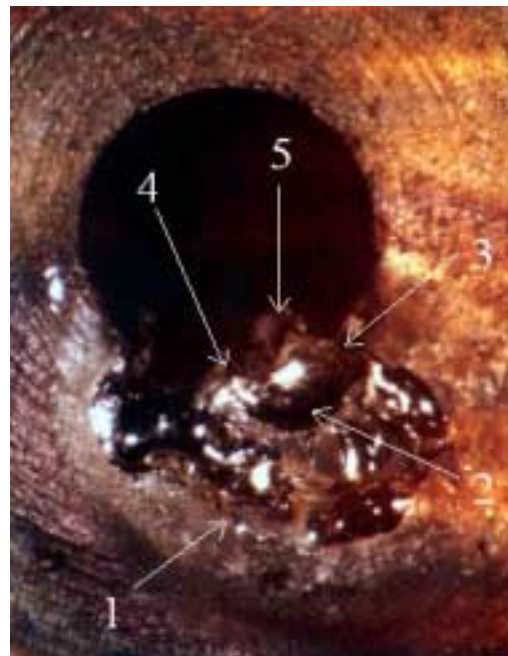
4.3.2.2: Molybdenum

Despite being tested for a full five minutes, the molybdenum anodes showed only slight surface damage. Figure 4.2a shows a black and white (for detail) photograph of molybdenum-1. Two distinct cavities (1 and 2) exist that are mostly filled with beads of molybdenum (3). It appears that, rather than being vaporized, the molybdenum remained liquid and recrystallized after the arc was extinguished. Also, the formation of double-cavities was quite rare, since the arc tended to stay attached to a single spot. During the test, the plasma jet was seen to whip back and forth like an agitated cat's tail, indicating

that the arc was constantly switching its attachment point back and forth between these two regions. Despite this unsteadiness, the jet appeared quite stable and did not sputter. As with tungsten-copper-2, some dripping back into the constrictor occurs (4). Although not clearly evident in this photo, there is also a spire (5) on the edge of the constrictor formed by through convection. A thread-like structure also appears in the constrictor exit (6), which is a small bit of molybdenum that has flaked off of the constrictor wall. Finally, there are two lobes of heat treatment removal around the edges of the two cavities (7), centering on the two separate arc attachment points.

A more characteristic landscape of a worn molybdenum anode is shown in Figure 4.2b. As was common with most anodes, there is one cavity (1), indicating a single arc attachment point. The cavity here is slightly larger than either of those shown in Figure 4.2a. As with Figure 4.2a, the cavity is filled with molybdenum beads (2). Also two spires bordering the constrictor exit have been formed from convective forces interacting with the molten molybdenum (3 and 4). Again, as with the molybdenum-1 and the tungsten-copper-2, there are drips (5), which originate at the base of the shallow cavity and extend into the constrictor. Surprisingly, heat treatment removal does not seem severe in this case, even though the arc was attached to the same location for five minutes.
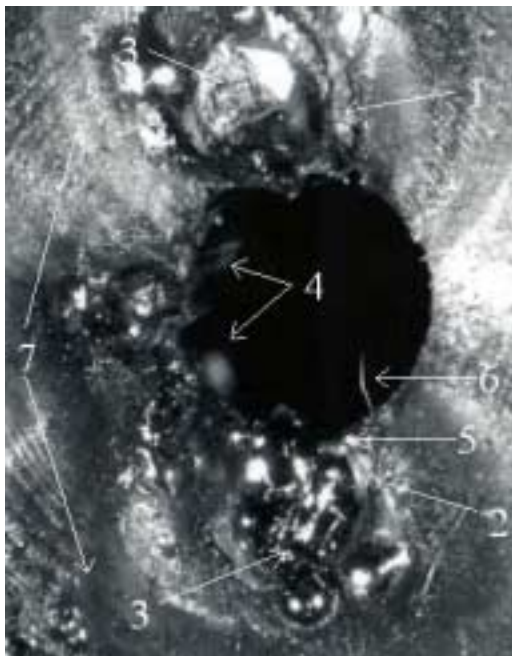
(a) Molybdenum-1   (b) Molybdenum (2)

Figure 4.2: Stereoscopic Photographs of Worn Molybdenum Anodes

4.3.2.3: Copper

Unlike the denser anode materials, pure copper anodes showed fewer identifiable features because the copper tended to be vaporized by the arc rather than melted and rearranged into spires or other features. Images of copper-1 appear in Figure 4.3 showing a large area of heat treatment removal (1) and a single, deep cavity (2). The path of heat flux can be seen to originate at the point of arc attachment and propagate outward, wrapping around the constrictor exit and forming a heart-shaped area of heat treatment removal. Close analysis of the cavity shows evidence that the arc attachment point was not stationary during this test. Five distinct parallel arcing grooves, ending in beads of copper (3) are shown in Figure 4.3b, indicating the paths the arc traveled during the test. The center groove is labeled.

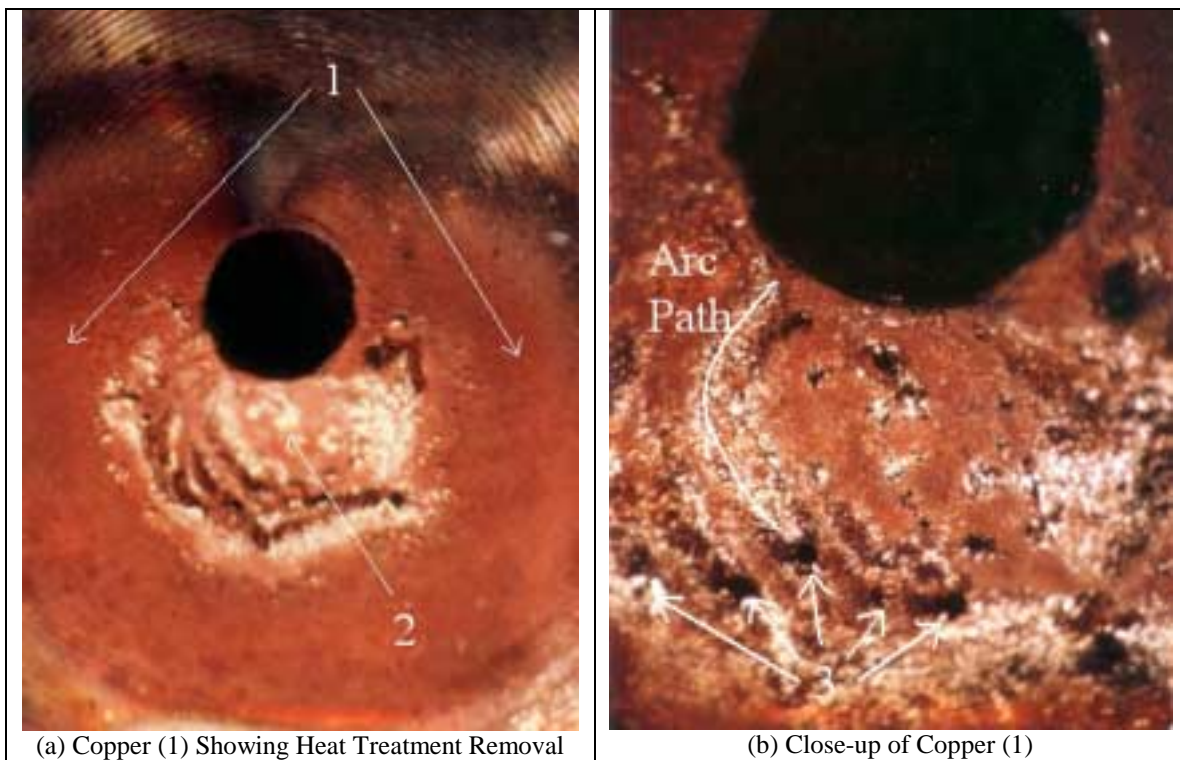| (a) Copper (1) Showing Heat Treatment Removal | (b) Close-up of Copper (1) |

Figure 4.3: Stereoscopic Photographs of Copper-1

A photograph of copper-3 is shown in Figure 4.4. From the stereoscopic investigation the material loss does not seem severe, supporting the experimental results that reported a loss of only 4 mg. Here no identifiable cavity exists, although a portion of the constrictor exit has been eroded (1). In addition, two spires (2 and 3) are located near

the constrictor exit, neither of which is very tall. The heat treatment removal is centered on the one closest to the constrictor (2) due to the pattern of discoloration and indicates the point of arc attachment. An interesting observation was made of a silver colored formation just inside the constrictor (4). It appears that this formation is a bead of tungsten from the tip of the cathode, which was deposited just before exiting the anode constrictor.
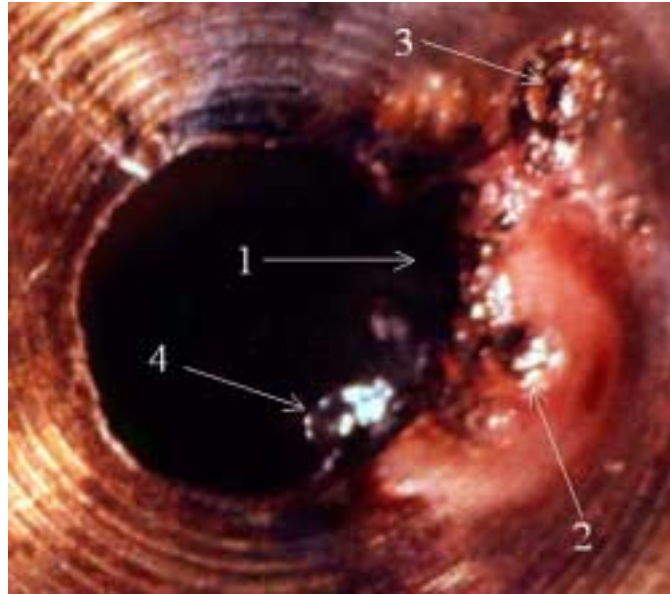

Figure 4.4: Stereoscopic Photograph of Copper-3

4.3.2.4: Investigations of the Cathode

In addition to the anode studies presented above, the cathodes of each test were also analyzed. From the values presented in Table 4.3, the average volumetric loss rate is 9.2 mm^3/sec, corresponding to an erosion rate of 1.1 mg/min. This value seems to be independent of run time or power, indicating that the cathode tip burns off almost immediately and then continues to slowly erode.

A microscopic investigation of the cathode tips after each run revealed a variety of wear patterns. Figure 4.5a is a picture of a new cathode for reference; whereas Figures 4.5b, c, and d show a variety of cathode tip wear patterns. Normal wear was indicated by a blunted tip as shown in Figure 4.5b, which corresponds to an even distribution of arc attachment about the tip region. Occasionally, other patterns were noticed, such as slanted tips or irregular shaped tips indicating the arc movement was not uniform about

the cathode. Examples of these are shown in Figures 4.5c and 4.5d, respectively. Slanted tips are formed by misalignment of the cathode, causing the arc to favor the side closest to the anode attachment point. Irregular surfaces, such as in Figure 4.5d, were quite rare and could have been caused by irregularities within the material itself.

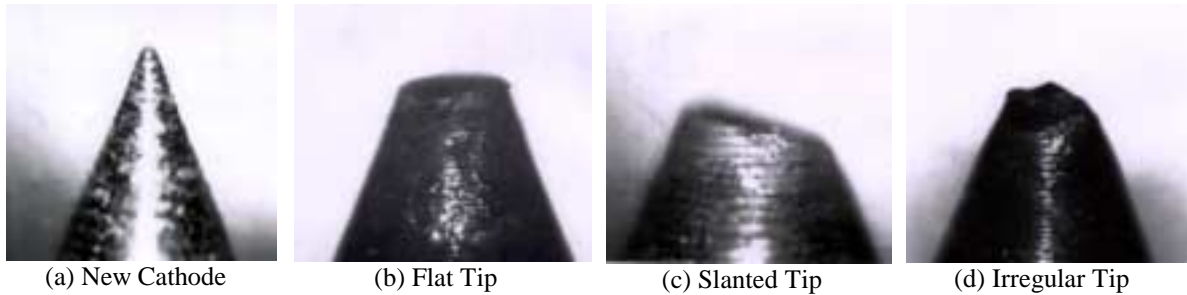| (a) New Cathode | (b) Flat Tip | (c) Slanted Tip | (d) Irregular Tip |

Figure 4.5: Microscopic Photos of Cathode Tip Wear

In addition to the microscopic investigation, the average current density for each test was calculated by measuring the cathode tip diameter and arc current. The average diameter of the cathode tips after testing was 0.90 mm. These rough estimates were taken with Venire calipers. For a current of 23 A, the average current density was calculated to be 3500 ± 400 A/cm^2. However, this method is not necessarily accurate, since the cathode spot might move and thereby produce a wear area larger than the arc area, causing an underestimation of the current density. A more realistic value may be as high as 7000 A/cm^2, assuming the arc fills half of the active area during testing.

4.3.3: The Anode Attachment Point Model

An analytical model was developed to determine how various anode material properties affect the area of arc attachment on the anode, and also to aid in interpreting the experimental results. Four materials were considered: molybdenum, copper, a 70/30 tungsten-copper alloy, and pure tungsten as a comparison, even though it was not included in the experimental tests because of its poor machineability. For a given current, the heat flux to the anode is greater for smaller-diameter arcs. Therefore, it would be beneficial to choose a material with a mix of material properties that would produce the largest arc diameter, and hence, reduce the rate of electrode erosion. The model allows for changes in the thermionic work function, arc current, and anode

operating temperature and thermal conductivity, in order to evaluate the effect these properties have on the arc diameter, d_a. The importance of each of these parameters is discussed below. The model consists of

$$\dot{S}_s = \dot{Q}_a\left(\frac{1}{T_a} - \frac{1}{T_p}\right), \tag{4.1}$$

$$\dot{Q}_a = I\phi_a + \xi IV_{af} + \pi\frac{d_a^{\,2}}{4}\left[h(T_p - T_a) + k_e\frac{(T_p - T_a)}{\delta} + \sigma\varepsilon(T_p^{\,4} - T_a^{\,4})\right], \tag{4.2}$$

$$\dot{Q}_a = k_a\pi\frac{d_a^{\,2}}{4}\left(\frac{T_a - T_c}{t}\right), \tag{4.3}$$

and

$$\frac{\partial\dot{S}}{\partial d_a} = 0; \tag{4.4}$$

and is based on a fundamental understanding that an arc will arrange itself in such a way as to minimize entropy production, $\dot{S}_s$, and heat transfer to the anode, $\dot{Q}_a$ (Mahan, 1998). For steady-state operation, an equal amount of heat is lost by conduction to the anode support, convection to the surrounding gases, radiation, and vaporization of the anode material, the latter being the effect most necessary to minimize. These effects are accounted for in Equation 4.2 and Equation 4.3.

For this analysis, k_e, the thermal conductivity of the electrons in the anode fall region, was assumed to be essentially the same as the conductivity of the anode metal at room temperature. The anode operating temperature was assumed to be 70% of the melting temperature of the anode surface. In addition, material properties for the 70/30 tungsten-copper alloy were not available from the manufacturer and so were interpolated from the pure metal properties in the 70-30 ratio. The values used for the model are listed in Table 4.4. Material properties for tungsten, molybdenum, and copper were taken from Smithells (1967).

Table 4.4: Model Parameters and Values

Variable	Description	Value/Units	100-W	100-Mo	100-Cu	70W/30Cu
T_p	Temperature of plasma	6,000 K				
T_c	Temperature of coolant	298 K				
ε	A multiplication factor	1.0				
ξ	A multiplication factor	1.0				
V_{af}	Voltage across anode fall	20 V				
h	Heat transfer coefficient	125 W/mK				
δ	Thickness of anode fall	0.001 m				
σ	Boltzmann's constant	5.67E-8W/(m^{2}K^4)				
t	Anode thickness	0.001 m				
I	Arc current	15-100 A				
ϕ_a	Thermionic work function	Volts	4.54	4.15	4.38	4.49
k_e	Conductivity at melting	W/mK	94.2	84.0	247	140
k_a	Conductivity at room temp.	W/mK	167	144.3	399	237
T_a	Anode operating temp.	K	2555	2010	950	2070

The thermionic work function of a metal is the work in volts necessary to remove a unit charge of electrons from the surface. This concept can be explained using the Shih equation,

$$q_e = j\left[\frac{5kT_e}{2e} + V_{af} + \phi_a\right]. \tag{4.5}$$

Equation 4.5 demonstrates the amount of heat transfer at the point of arc attachment, q_e, and is a function of the thermal energy of the electrons (first term), kinetic energy gained by electron acceleration through the anode fall region (second term), and the kinetic energy given up by the electrons on impact (third term, where ϕ_a is the thermionic work function of the anode). It is important to note that each term is multiplied by the current density, j. Since we are only interested in the on-impact effects the equation can be reduced to

$$q_e = j\phi_a. \tag{4.6}$$

From this simplified version of the Shih equation, it is quite clear that increasing the thermionic work function means that, for a constant current, a reduction in current density must occur (i.e. the arc will expand) to minimize the heat transfer to the anode.

In addition to a high thermionic work function, elevated anode operating temperatures are also desirable for increasing the arc diameter. According to equation 4.2, a high operating temperature decreases the heat transfer from the plasma to the anode through convection, electron energy exchange, and radiation. Through coupling with

other equations in the model, this causes the arc diameter to increase. This concept is intimately linked with the thermal conductivity of the anode material. Low thermal conductivities would cause higher anode operating temperatures and hence a larger arc attachment point.

As with the high operating temperatures, a low thermal conductivity within the anode fall region, k_e, is also desirable. According to the Lorentz ratio,

$$L = \frac{\sigma_e}{k_e},$$ (4.7)

as the thermal conductivity, k_e, of an electron gas decreases, the electrical conductivity, σ_e, must also decrease to maintain a constant ratio. Consequently, it is also known that as the electrical conductivity of an electron gas decreases, the charge concentration must also decrease (i.e. the arc expands) (Papoular, 1963).

Finally, as current increases, the net effect is that the arc must expand, or reduce its resistivity to maintain a constant voltage. In actuality, both occur. The centerline of the arc reaches a higher temperature, reducing the resistivity of the arc; and the arc expands to accommodate the larger number of electrons passing through (Stouffer, 1989). Although increased currents will naturally cause a higher rate of electrode erosion, it will be shown that the model predicts that the arc diameter increases with current, as it should.

The results of the analysis for the four anode metals are presented in Figure 4.6. As expected, the predicted arc attachment diameter for tungsten is by far the largest, indicative of a lower anode erosion rate. Molybdenum and the tungsten-copper alloy were somewhat equal, with molybdenum producing a slightly larger arc diameter for the current range. The model predicted copper had the highest erosion rate because it produced narrower arcs due to its high electrical and thermal conductivities. At higher currents, the difference in arc diameter among the materials increases, indicating that the erosion rate of copper would increase at a much faster rate than for the other materials.
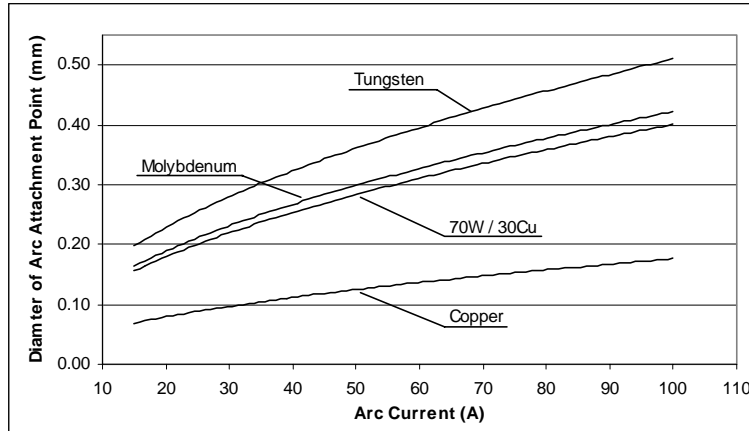
Figure 4.6: Results of Analytical Arc Diameter Analysis

This model predicts the trends of the anode material performance observed in the experimental tests quite well. The experimental results showed that the molybdenum and the tungsten-copper anodes had much lower volumetric losses than the pure copper anodes. If the arc diameter predicted by the model were directly proportional to the volumetric material loss, then one would expect the volumetric loss for copper anodes to be about two times as great as that of molybdenum or tungsten-copper. In comparison to the experimental results, the model slightly under predicts this trend. Referring to Table 4.2, the volumetric losses of the pure copper anodes to the molybdenum and tungsten-copper anodes were respectively 2.5 and 3.5 times as great. However, the low number of anodes tested could easily explain this difference and is the reason this model was needed to supplement the experimental work. Essentially, the analytical model and the experimental results are in close agreement regarding the anode material of choice, molybdenum.

## 4.3.4: Crossflow and Anode Exit Geometry Effects on Arc Attachment Point

The effect of crossflow and anode exit geometry had a profound effect on the location of the arc attachment point. The flow swirler within the torch was designed to force the arc to rotate about the cathode tip and anode exit, thus reducing electrode erosion rates. However, when introduced into a supersonic crossflow, the crossflow tended to negate the effects of swirl at the anode exit and forced the arc to attach either on the downstream side of the anode constrictor or on the side of the anode constrictor where the swirl velocity component and the crossflow velocity component were in

opposite directions. Once the arc attached to the anode, the arc would almost always reattach in that same location in subsequent tests. On very rare instances, the arc would be observed to switch attachment points.

4.3.4.1: Arc Attachment for Normal Injection

For almost all tests involving normal injection (perpendicular to the crossflow), the arc was observed to attach on the downstream side of the constrictor exit. In a few instances, the arc would attach on the side of the constrictor where the velocity components of the swirl and crossflow were in opposition to one another. A photograph of a molybdenum anode used in the supersonic tunnel is shown in Figure 4.7, where flow is from left to right. This particular anode was started over 50 times, with test durations of 10 seconds and an average power of approximately 2000 W. The photograph shows that the arc reattached in the same spot each time the torch was started, but also demonstrates the robustness of using molybdenum as an anode material. The following is a short discussion of some of the major features present within the photograph and their importance in understanding the behavior of arcs in supersonic crossflow.

The most identifiable feature in Figure 4.7 is the presence of a large mound (1), approximately 1 mm high, formed from recurring arc attachments on the downstream side of the anode constrictor. The molybdenum in this region was repeatedly melted, flowed up out of the constrictor and into the crossflow, and then cooled after the torch was turned off. Two cracks, caused by constant recrystalization and thermal loading of the material, can be seen on the constrictor face of the mound (2). Two smaller mounds (3 and 4) were formed on the outer edges of the large mound and are approximately 0.5 mm high. Heat treatment removal is evident by the discoloration of the molybdenum (5) around the entire formation, and centers on the arc attachment point. Downstream of the large mound (1), a soot trail has been deposited on the anode surface (6). In addition, evidence of what are believed to be molybdenum nitride and oxide deposits appears just downstream of the mound in a recirculation zone (7 and a close-up in Figure 4.7b). These white and blue crystalline formations have the appearance of cauliflower and are unique to this anode.
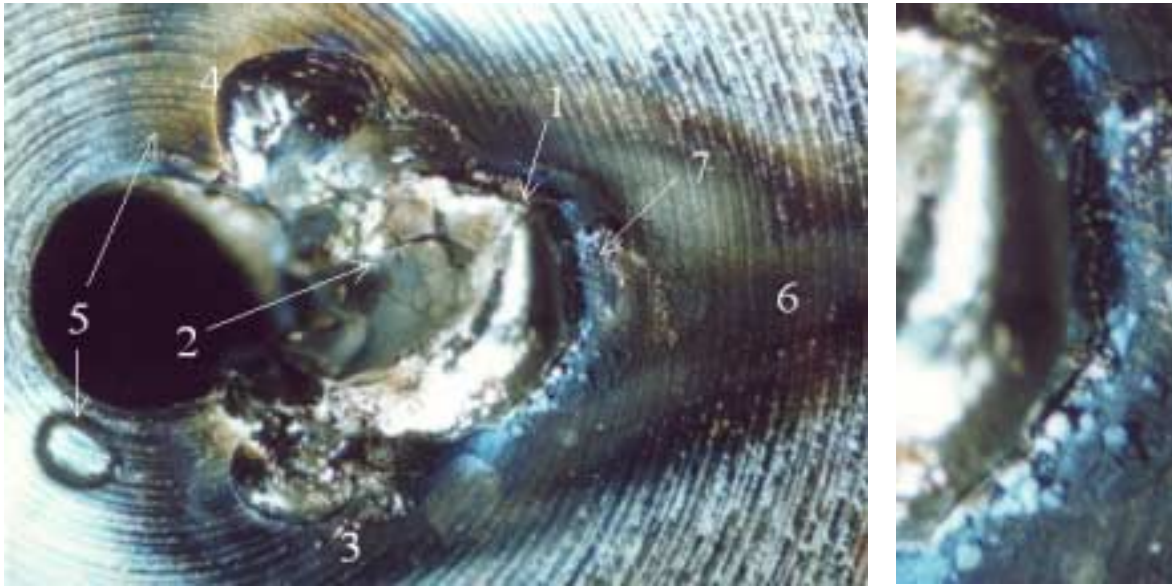
(a) Photograph of Molybdenum Anode Features   (b) Close-up of Crystals
Figure 4.7: A Molybdenum Anode in Crossflow after 50+ Runs
(Scale: Constrictor Exit Diameter = 1.59 mm)

4.3.4.2: Arc Attachment for Angled Injection

The anode exit geometry was observed to have a noticeable, if not always predictable, effect on the arc attachment point. Anodes designed for angled injection have an elliptical constrictor exit, allowing flush-walled injection of plasma, as shown in Figure 4.8. The arc attachment point differed from that with anodes designed for normal injection, in that the arc was never observed to attach on the downstream side of the constrictor. Rather, the arc would attach on the upstream side of the constrictor at the point of attachment allowing the shortest arc length. Furthermore, the anode geometry at this point also produces a concentration in the electric field due to the low radius of curvature, allowing easier ionization of the gas and a tendency of the arc to follow this path. In some cases the arc would also attach on one of the sides perpendicular to the crossflow. In addition, the arc attachment point was usually not static. On a number of occasions, the arc was observed to switch positions; this usually occurred when the arc eroded the upstream portion of the anode constrictor.
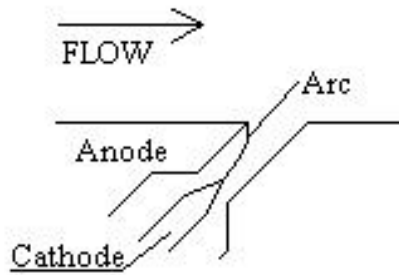
Figure 4.8: A Schematic of an Anode Designed for Angled Injection

Two examples of anodes used for angled injection are shown in Figure 4.9, where crossflow is from top to bottom. The anodes here are made from copper and were designed for 45° angled injection. In Figure 4.9a, the arc attachment point appears to have attached mainly on the right side of the exit (1), but evidence of anode wear is also seen on the upstream side and, to a lesser extent, on the left side of the exit. The area of most intense arc attachment (1) shows a smooth, crater-like structure. The copper bead (2) on the left side of the anode exit was once molten and was pushed downstream by the crossflow, whereupon it cooled once the torch was turned off. This run-off was much more common with angled anodes than with normal injection. Arc attachment on the upstream side has eroded a portion of the anode exit (3), leaving nonuniformity in the exit flow region. This was a problem identified with angled anodes, as the wall thickness in this region is thinner than for other portions of the constrictor. Premature erosion of this area was observed to change the shape of downstream total temperature profiles.

The second copper anode used for angled injection, shown in Figure 4.9b, exhibited arc attachment exclusively on the left side of the anode exit. Molten run-off is evident here as well. The erosion here is not quite as severe, even though the arc attachment point appears to be in only one place. The main point to be made from these two photos is that it was clear that the location of the arc attachment point was unpredictable, and often moved, due to the elliptical exit geometry.
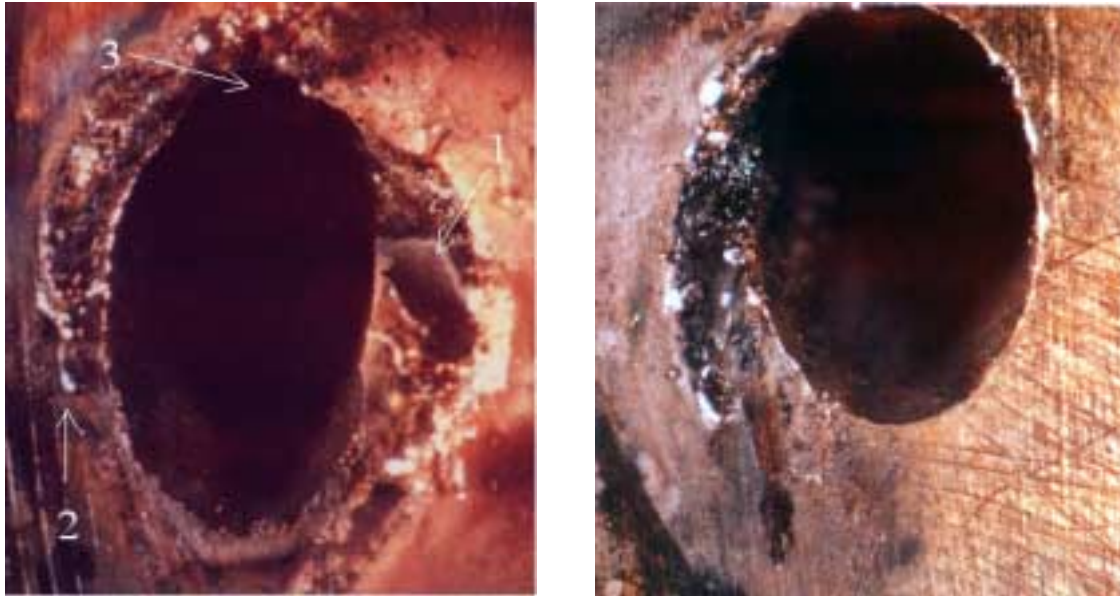
(a) Anode #1, Copper, 45° Angled Injection   (b) Anode #2, Copper, 45° Angled Injection

Figure 4.9: Wear on Copper Anodes for 45° Angled Injection

4.3.5: The Effect of Air and Nitrogen Plasmas On Molybdenum

The purpose of the experiments presented in this chapter was to determine what material would be best suited as a replacement for tungsten and to determine how exit geometries affected the wear rate of the material. However, it was discovered that air and nitrogen plasmas were quite erosive to molybdenum, so erosive that the molybdenum anodes became almost worthless when testing with these feedstock gases. Molybdenum anodes operated well with hydrocarbon plasmas, much better than copper anodes did; but when air or nitrogen feedstocks were used, the anode lifetime decreased considerably. Copper anodes, on the other hand, proved their merit by acting as a satisfactory replacement for molybdenum when these feedstocks were used.

Stereoscopic photos of two molybdenum anodes after testing with nitrogen and air feedstocks are shown in Figure 4.10. The anode in Figure 4.10a was used in six tests, each lasting about 10 seconds. The amount of mass loss in this span of time is severe, with the wear evident on the surface extending deeply into the anode constrictor. Five separate identifiable arc attachment points exist (1a-e), indicating that the arc attachment point was unstable as the plasma eroded the anode material. A single portion of the constrictor exit was not eroded (2), which was quite surprising given the test durations. Also, the presence of a gray-silver powder covering a majority of the anode surface

indicates evidence of molybdenum-air interactions by. This powder, believed to be molybdenum nitride, is discussed in more detail in Chapter 5. As a final note, the lack of spires, or beads of molybdenum deserves mention. The absence of these formations, as seen with earlier hydrocarbon tests, shows that once the arc melts the molybdenum, the molten molybdenum interacts with the air plasma to form crystalline molybdenum compounds. These compounds are then carried away by convection.

The molybdenum anode shown in Figure 4.10b was operated for about one second after the high-frequency burst with air as the feedstock. The amount of erosion for this time duration is quite severe, and cannot be wholly attributed to start-up phenomena. The damage is contained primarily on one side of the constrictor (1) and extends almost all the way back to the constrictor entrance. More noteworthy is the slight wear evident on the opposite side of the constrictor (2), which does not seem to have been caused by the arc, but rather by interaction with the plasma. Even for such a short burst, evidence of heat treatment removal (3) around the arc attachment point is present.
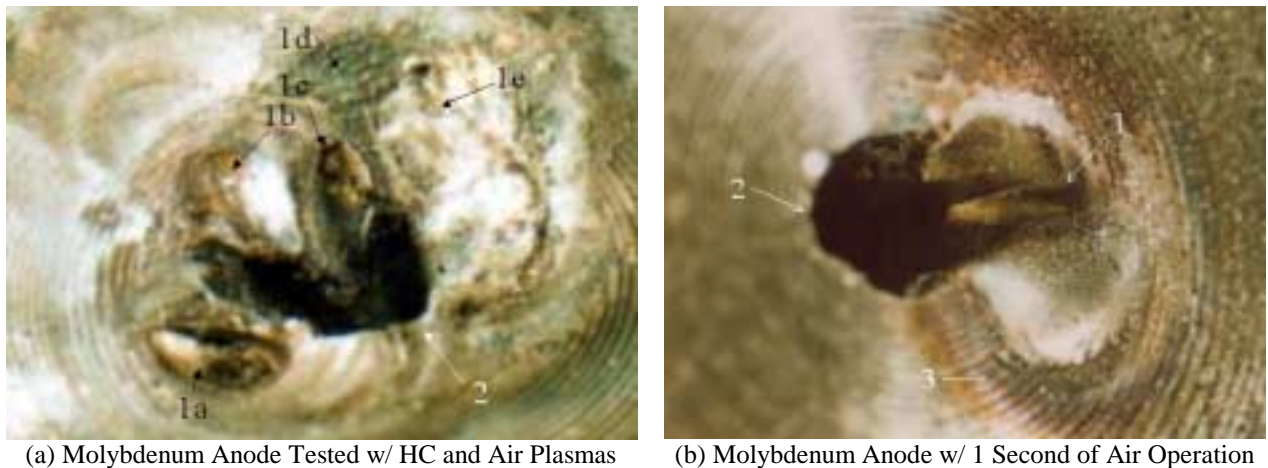

(a) Molybdenum Anode Tested w/ HC and Air Plasmas   (b) Molybdenum Anode w/ 1 Second of Air Operation

Figure 4.10: Molybdenum Anodes Showing Erosion from Air Plasma

4.4: Conclusions

Five electrode erosion studies were presented in this chapter. An experimental volume-loss study and an arc diameter model were used to select a new anode material, since the anode design for VTPT-3 is too large and complex to be machined from tungsten. Two stereoscopic investigations of worn anode surfaces showed how

supersonic crossflow and elliptical exit geometries affect the arc attachment location. In addition, a study of the erosive effects of nitrogen and air plasmas on molybdenum was conducted.

The quiescent experiments involved measuring the volumetric losses for three different anode materials: molybdenum, copper and a tungsten-copper alloy. Tungsten-copper alloys experienced the lowest volumetric loss rate, but molybdenum anodes demonstrated longer lifetimes and better stability. Copper anodes performed poorly, having the highest volumetric loss rates and shortest operational lifetimes. The arc diameter model agreed well with the experimental results, in that, of the materials tested, molybdenum would be the best replacement for tungsten. The analysis predicted the diameter of the arc attachment point for different anode materials, which is an indication of the rate at which material would be vaporized. Larger arc attachment points are desirable.

Stereoscopic analyses were conducted to provide a better understanding of arc attachment points in a quiescent environment, and also to explain how the addition of a crossflow and elliptical exit geometry affect the location of attachment. Close examination of the anode surfaces showed evidence of anode erosion such as cavities and arc path grooves. Convective forces near the constrictor exit also formed short spires and drip formations out of the molten metals as they cooled. When introduced into a crossflow, experimental observations revealed that the preferred location of arc attachment was on the downstream side of the constrictor. Occasionally, the arc would attach on the side of the constrictor where the swirl velocity, induced by the flow swirler, and crossflow velocity components were opposed. Elliptical exit geometries used for angled injection also profoundly affected the arc attachment point. In these cases, the arc was observed to attach either on the upstream side of the constrictor, producing the shortest arc length, or on the sides of the constrictor where the swirl was negated by the crossflow. The arc attachment point for these geometries was less predictable than for the normal injection cases.

Tests with nitrogen and air feedstocks showed that the plasmas from these feedstocks were quite erosive to molybdenum. Spectroscopic analysis of molybdenum anodes showed erosion from these feedstocks occurred quickly and severely reduced the

operational lifetime of molybdenum anodes. Therefore, with these feedstocks, copper, which exhibited good resistance to these erosive plasmas, was used in place of molybdenum.